Electronic Supplementary Information

Anodic Electrogenerated Chemiluminescence Behavior and the Choline Biosensing Application of Blue Emitting Conjugated Polymer Dots

Hongmei Chen, Qiyi Lu, Jiayao Liao, Ruo Yuan and Shihong Chen*

1 Experimental

1.1 Reagents and chemicals

The polyfluorene derivative poly (9,9-dioctylfluorenyl-2,7-diyl) (PFO, MW 147000, polydispersity 1
O_2, C_{60} were obtained from Aladdin Ltd. (Shanghai, China). Toluene, tetrahydrofuran (THF), choline chloride, and choline oxidase were obtained from Sigma Chemical Co. (St. Louis, MO, USA). Polyamidoamine (PAMAM, generation 5) was purchased from Weihai CY Dendrimer Technology Co., Ltd (Weihai, China). Phosphate-buffered saline (PBS) solutions with different pH were prepared with 0.10 M Na_2HPO_4 and 0.10 M KH_2PO_4 (containing 0.10 M supporting electrolyte KCl). The human serum samples were gotten from the 9th People's Hospital of Chongqing. Ultra pure water was used throughout the whole experimental process. All other chemicals were of analytical grade without further purification.

1.2 Apparatus

*Corresponding author **Tel:** +86-23-68253172 **Fax:** +86-23-68253172

E-mail address: cshong@swu.edu.cn. (S.Chen)

The ECL emission was monitored by a MPI-E electrochemical analyser (Xi'an Remax Analyse Instrument Co. Ltd, Xi'an, China) in PBS (0.10 M, pH 7.0) with the voltage of the photomultiplier tube (PMT) set at 800 V in the detection. Cyclic voltammetry (CV) and electrochemical impedance spectroscopy (EIS) measurements were performed with a CHI 600D electrochemical work station (Shanghai Chenhua Instruments Co., China) in 3.0 mL 0.10 M PBS (pH 7.0) containing 5.0 mM $K_3[Fe(CN)_6]/K_4[Fe(CN)_6]$. Fourier transform infrared spectroscopy (FT-IR) was performed on an IFS 66 V/S (Bruker) IR spectrometer in the range of 400~4000 cm^{-1}. Fluorescence spectrometry was performed on a FR-5301-PC spectrophotometer (Shimadzu, Tokyo, Japan) at room temperature with the range of 420~550 nm. The UV-visible (UV-vis) spectrometry was performed on a Lambda 17 UV-vis spectrometer 8500 (PECo., USA) with the range of 200~600 nm. The morphology and size of various nanomaterials were analyzed using a scanning electron microscopy (SEM) (SEM, S-4800, Hitachi, Japan) with an acceleration voltage of 10 kV. The fluorescent photos were gotten by UV transilluminator (Shanghai clinx Science Instruments Co., CUV 10).

1.3 Preparation of PFO Dots

PFO dots were synthesized according to the literature[1] with some changes. In brief, 4 mg of PFO was dissolved in 2 mL of THF by stirring overnight at the room atmosphere. The mixture was filtered with a 0.7 m glass fiber filter to remove insoluble material. Subsequently, 8 mL of water was added into the solution to prepare the polymer dots. Then, THF was removed by partial vacuum evaporation.

After a small fraction of aggregates were removed through twice centrifugation at 6000 rpm for 5 min, the obtained PFO dots were dispersed in 4 mL ultra pure water.

1.4 Preparation of C_{60}-PAMAM

Firstly, C_{60} aqueous solution was prepared via a phase-transfer method by adding C_{60} toluene solution into ultra pure water. Simply, 5.0 mL C_{60}-toluene solution (1 mg/mL) was mixed with 2.5 mL ultra pure water by ultrasound. Then, 4 mg of PAMAM was dissolved in 1 mL of ultra pure water to get 4 mg/mL PAMAM solution. Subsequently, 5 μL PAMAM (4 mg/mL) and freshly prepared 500 μL C_{60} aqueous solution (2.5 mg/mL) were mixed together with ultrasound to form positively charged C_{60}-PAMAM nanocomposite with affluent amino groups.

1.5 Preparation of C_{60}-PAMAM-PFO

In this work, the C_{60}-PAMAM-PFO nanocomposite was prepared through electrostatic adsorption between the negatively charged PFO dots and positively charged C_{60}-PAMAM. The above prepared C_{60}-PAMAM (500 μL) and PFO dots (1.5 mL) were mixed by ultrasound, followed by centrifuging and washing twice with water to get C_{60}-PAMAM-PFO nanocomposite. The prepared C_{60}-PAMAM-PFO was dispersed in ultra pure water and stored at 4 °C when not used. The preparation process of C_{60}-PAMAM-PFO composite was illustrated in Scheme 1.

1.6 Preparation of the modified electrodes

Firstly, a glassy carbon electrode (GCE, Φ=4.0 mm) was sequentially polished

with 0.3 μm and 0.05 μm alumina slurries and ultrasonically cleaned in ethanol and water. 20 μL of C_{60}-PAMAM-PFO dispersion was cast onto the surface of cleaned GCE and air-dried at room temperature to get C_{60}-PAMAM-PFO/GCE. Then 8 μL of Chox solution (100 U/mL) was further modified onto the C_{60}-PAMAM-PFO/GCE to prepare the biosensor (Chox/C_{60}-PAMAM-PFO/GCE). The fabrication process of the biosensor was illustrated in Scheme 1. For a control experiment, C_{60}-PAMAM/GCE, PFO/GCE, C_{60}-PFO/GCE, and PAMAM-PFO/GCE were prepared through dropping 20 μL of corresponding solution onto the surface of a cleaned GCE.

1.7 Experimental determination

The SEM images were collected as the following steps. Firstly, the dispersion of different nanomaterials was dropped onto the silicon wafer and dried at the room temperature. Then, the modified silicon wafers were used to perform the SEM measurements, thus achieving corresponding SEM images. During this process, the samples wasn't coated with a metal layer.

The EIS and CV measurements were performed in 3.0 mL 0.10 M PBS (pH 7.0) containing 5.0 mM $K_3[Fe(CN)_6]/K_4[Fe(CN)_6]$ (1:1). The ECL detection was performed in 3.0 mL 0.10 M PBS. The whole measurement process was supported by a conventional three electrode system at the room temperature. A modified GCE was used as working electrode, a platinum wire as auxiliary electrode, and a saturated calomel electrode (SCE) as reference electrode for electrochemical measurements and Ag/AgCl (saturated KCl) as reference electrode for ECL detection. The ECL

determination was based on the change in ECL intensity ($\Delta I = I_t - I_0$). Herein, I_t and I_0 are the ECL signals with and without the substrate, respectively.

2 Results and discussion

2.1 Characterization of nanomaterials

UV-Vis absorption spectroscopy was used to identify the formation of C_{60}-PAMAM-PFO nanocomposite and the results were shown in Fig. S1A. For PFO (curve a), a peak at 408 nm was observed, which was attributed to the π-π* transition of the fluorene units. The peak at 435 nm was due to the formation of polyfluorene's crystalline β phase. Additionally, an absorption peak of PFO was observed at 205 nm, which was caused by the π-π* transition of the aromatic compound. For C_{60} (curve b), three strong optical absorption peaks were observed at 218, 263 and 344 nm, respectively. For C_{60}-PAMAM (curve c), two absorption peaks at 229 nm and 286 nm were ascribed to PAMAM. Compared to C_{60}-PAMAM (curve c), the characteristic peaks of PFO were observed at 410 nm and 438 nm in C_{60}-PAMAM-PFO (curve d), indicating that C_{60}-PAMAM-PFO has been successfully prepared.

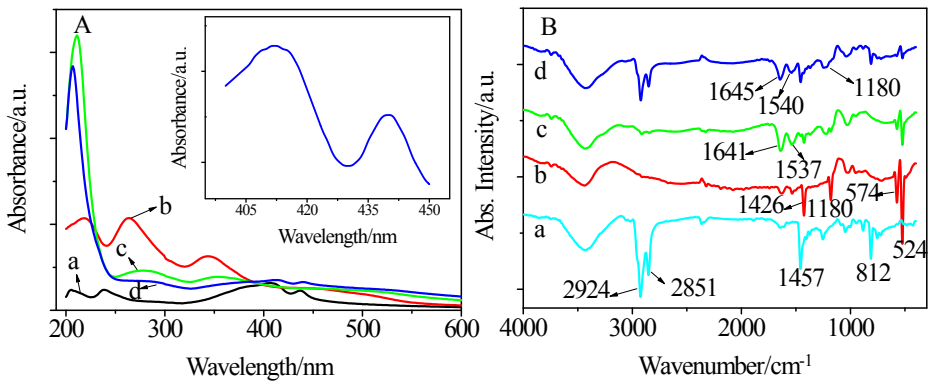

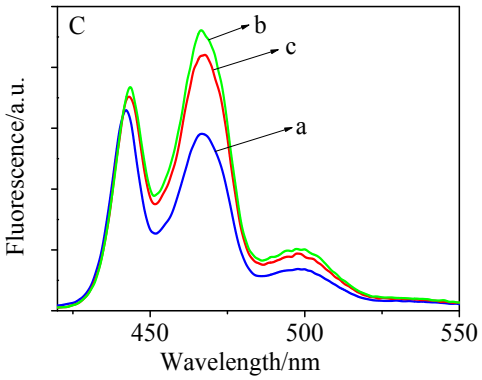

Fig. S1 (A) UV-vis absorption spectra and **(B)** FT-IR spectra of (a) PFO, (b) C_{60}, (c) C_{60}-PAMAM, and (d) C_{60}-PAMAM-PFO. The inset of Fig. S1A: the enlarged picture of curve d in the range of 400~450 nm. **(C)** The fluorescence spectra of (a) PFO dots and (b) C_{60}-PAMAM-PFO nanocomposite without H_2O_2. The fluorescence spectra of (c) C_{60}-PAMAM-PFO nanocomposite with 0.05 mM H_2O_2.

The FT-IR spectroscopy was also used to characterize the formation of C_{60}-PAMAM-PFO nanocomposite and the results were shown in Fig. S1B. For PFO (curve a), two peaks at around 2851 cm^{-1} and 2924 cm^{-1} were observed in the range of 2500~3000 cm^{-1}, which were due to the C–H stretching vibrations of the alkyl chain of PFO. The alkyl C–H rocking mode appeared at 812 cm^{-1}. The peak at 1457 cm^{-1} was assigned to the aromatic ring breathing vibration. For C_{60} (curve b), because of the typical dipole-allowed, the characteristic bands of C_{60} were observed at 524, 574, 1180 and 1426 cm^{-1}, respectively. Compared with C_{60} (curve b), C_{60}-PAMAM (curve c) appeared two new band peaks at 1641 and 1537 cm^{-1}, which were due to amides (–CO–NH–) I and II of PAMAM, respectively. In the case of C_{60}-PAMAM-PFO (curve d), all characteristic peaks of PFO, C_{60} and PAMAM could be observed. Furthermore, one amide (–CO–NH–) peak of PAMAM located at 1641 cm^{-1} red-shifted to 1645 cm^{-}

[1] and the other amide (–CO–NH–) peak of PAMAM located at 1537 cm^{-1} red-shifted to 1541 cm^{-1}, which might be affected by the aromatic ring of PFO. Above results indicated the successful preparation of C_{60}-PAMAM-PFO composite.

The fluorescence (FL) spectra also were performed and the results were shown in Fig. S1C, as observed, in the absence of H_2O_2, PFO dots (curve a) presented three well resolved vibronic peaks at 443nm, 468 nm and 497 nm, respectively, which were consistent with the previous reports[1]. Compared with PFO (curve a), the FL spectra of C_{60}-PAMAM-PFO (curve b) without H_2O_2 were almost unchanged. When H_2O_2 was added into the C_{60}-PAMAM-PFO dispersion (curve c), the FL spectra of C_{60}-PAMAM-PFO were also almost unchanged, compared to the case of without H_2O_2 (curve b).

In this work, the PFO dots were prepared by injecting PFO-THF solution into water to solve the poor water-solubility of PFO. In order to compare the water solubility of the PFO and PFO dots, 1 mg PFO and 1 mg PFO dots were dispersed in 2 mL ultra pure water with vigorous ultrasound for 10 min and then stayed 10 min, respectively. As shown in Fig. S2, the PFO dots (b) were dispersed in water uniformly, while the PFO was floated on the surface of the water (a). Obviously, the limitation of poor solubility of PFO would be well solved by using PFO dots instead of PFO for constructing sensors.

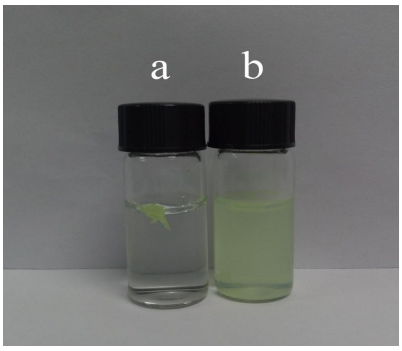

Fig. S2 The dispersity of (a) PFO and (b) PFO dots in water.

In order to investigate the reproducibility for preparing C_{60}-PAMAM-PFO composites from batch to batch, three batches of C_{60}-PAMAM-PFO composite were prepared and corresponding SEM images were shown in Fig. S3. As expected, the SEM images of different batches with the same synthetic method were analogous, indicating a good reproducibility for the preparation of C_{60}-PAMAM-PFO. What's more, the relative standard deviation (RSD) of ECL responses for three different batches was 1.46%, as shown in Fig. S4, suggesting that the effect of the variation in composition of C_{60}-PAMAM-PFO on the detection results was negligible.

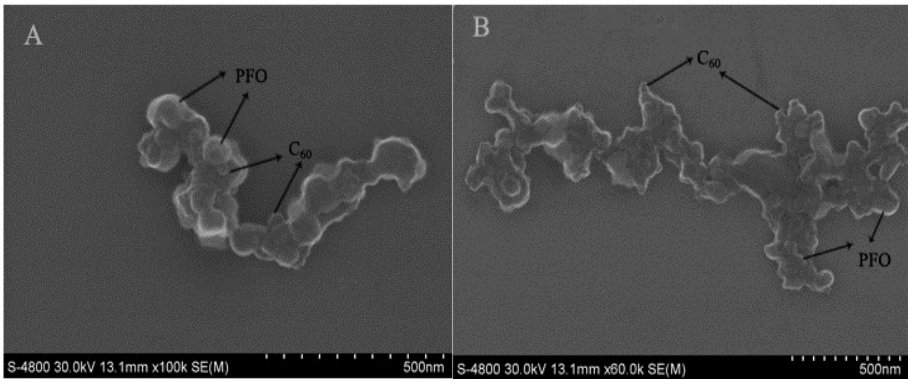

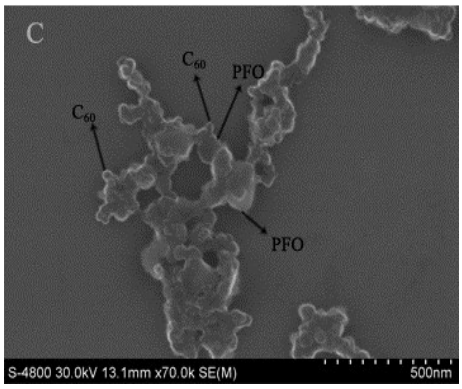

Fig. S3 SEM images of C_{60}-PAMAM-PFO modified films with three different batches.

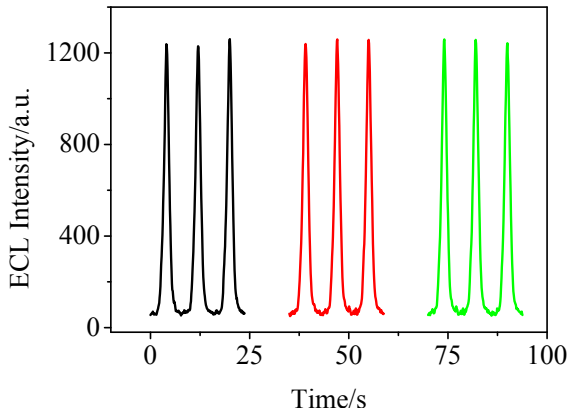

Fig. S4 The ECL responses of C_{60}-PAMAM-PFO/GCE to 3.50×10^{-8} M choline with three different batches in 0.10 M PBS (pH 7.0).

In addition, in order to more clearly identify the difference between the PFO dots and C_{60}, the ECL behaviours of C_{60}-PAMAM nanocomposite and PFO-C_{60}-PAMAM nanocomposite were studied. As expected, no ECL signal was observed at the ECL curve of C_{60}-PAMAM modified electrode (Fig. S5, curve a). However, for PFO-C_{60}-PAMAM modified electrode, an obvious ECL signal was observed at 1.97 V. Obviously, such an ECL signal resulted from the annihilation reaction of PFO. These results indicated that the successful synthesis of PFO-C60-PAMAM. These results

indicated that the successful synthesis of PFO-C_{60}-PAMAM, furthermore also can provide a strong evidence to identify the difference between the PFO dots and C_{60}.

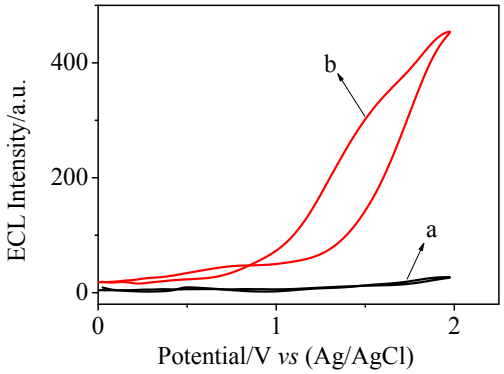

Fig. S5 ECL behaviors of (a) C_{60}-PAMAM/GCE and (b) PFO-C_{60}-PAMAM/GCE in 0.10 M PBS (pH 7.0).

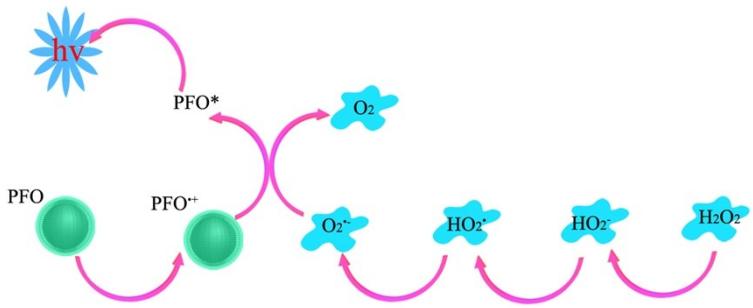

Scheme S1 Diagram of the ECL mechanism of PFO.

2.2 Optimization of experimental conditions

The influence of the pH of buffer solution in the ECL response of the biosensor was investigated and the results were shown in Fig. S6A. As seen, in the presence of 3.50×10^{-8} M choline, the change in ECL intensity (ΔI) at Chox/C_{60}-PAMAM-PFO/GCE increased with the increase of the pH from 5.5 to 7.0 and decreased after

pH 7.0, so the pH 7.0 was chosen as the optimal pH. Such an optimal pH may be ascribed to following reason. On the one hand, the pH would influence the ECL behavior of PFO-H_2O_2 system. On the other hand, the catalytic activity of Chox would be affected by pH.

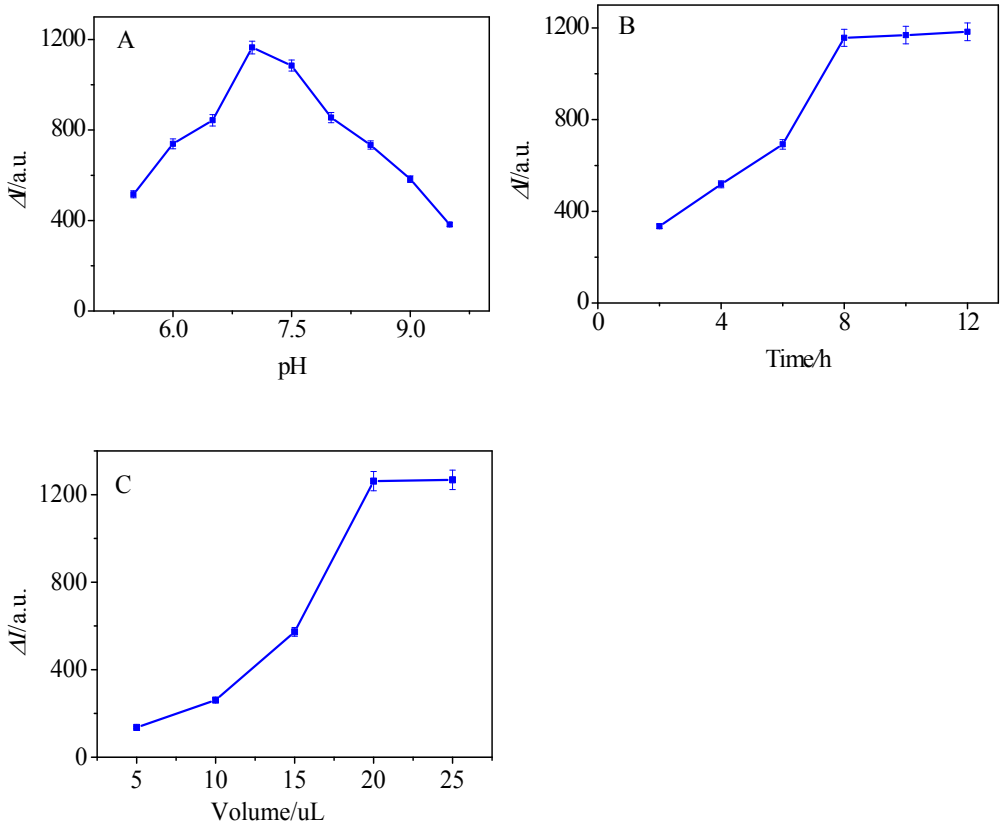

Fig. S6 Effect of **(A)** pH, **(B)** the incubation time of Chox and **(C)** the amount of C_{60}-PAMAM-PFO on ΔI at GCE/C_{60}-PAMAM-PFO/GCE to 3.50×10^{-8} M choline in 0.10 M PBS

The incubation time of Chox was also optimized since it would influence the quantity of the Chox modified on the electrode. The change of the ΔI at Chox/C_{60}-PAMAM-PFO/GCE with the incubation time of Chox was investigated and the results were shown in Fig. S6B. As seen, the ΔI increased with the increase in incubated time of Chox from 2 h to 8 h and reached a relatively stable platform over 8

h. Thus, 8 h was chosen as the incubation time of Chox.

Actually, the quantity of Chox on the electrode is dependent on the amount of C_{60}-PAMAM-PFO modified on the electrode, thus itself was optimized for the preparation of the biosensor. The optimal amount of C_{60}-PAMAM-PFO was achieved through detecting the change of ΔI at the biosensor with the volume of C_{60}-PAMAM-PFO dispersion modified on the electrode. As shown in Fig. S6C, the ΔI increased with the volume of C_{60}-PAMAM-PFO dispersion modified on the electrode in the range of 5~20 μL, and reached a platform after 20 μL. This may be due to the fact that C_{60}-PAMAM-PFO could improve the electro-active surface area of the modified electrode, thus further improve the quantity of Chox. In order to confirm this conjecture, the change of the electro-active surface area of the modified electrode with the volume of C_{60}-PAMAM-PFO deposited on the electrode was investigated. The cyclic voltammograms (CVs) of the modified electrode at different potential scan rates were recorded with 5.0 mM $K_3Fe(CN)_6/K_4Fe(CN)_6$ (1:1) as redox probes. Based on the relation between anodic peak current and square root of the scan rate, the electroactive surface area of the electrode (A) was calculated using Randles-Sevcik equation[2]

$$I_p=2.69\times10^5\times D^{1/2}\cdot C\cdot A\cdot v^{1/2}\cdot n^{3/2}$$

For 5 μL, 10 μL, 15 μL, 20 μL, and 25 μL of C_{60}-PAMAM-PFO dispersion, the electro-active surface areas of corresponding modified electrodes were 0.093 cm^2, 0.127 cm^2, 0.150 cm^2, 0.184 cm^2, and 0.186 cm^2, respectively. As expected, when the

volume of C_{60}-PAMAM-PFO dispersion increased from 5 μL to 20 μL, an obvious increase in electro-active surface area of the modified electrode was noticed. After 20 μL, further increase of the volume of C_{60}-PAMAM-PFO dispersion caused only a slight enhancement in electro-active surface area of the modified electrode. This result is consistent with that in the case of ΔI. Thus, 20 μL of C_{60}-PAMAM-PFO dispersion was chosen for the preparation of the biosensor.

2.3 Effect of C_{60} and PAMAM on the ECL response of the sensor

In order to investigate the effect of PFO, C_{60} and PAMAM on the PFO-H_2O_2 ECL system, the ECL behaviors of different modified electrodes were compared under the scanning potential in the range of 0~2.0 V, and the results were shown in Fig. S7. As seen, compared with the bare GCE (curve a), PFO/GCE (curve b), C_{60}-PFO/GCE (curve c), and PAMAM-PFO/GCE (curve d), the target sensor (C_{60}-PAMAM-PFO/GCE) showed the maximum ECL intensity, indicating that both C_{60} and PAMAM exhibited a promoting effect on the ECL intensity in PFO-H_2O_2 ECL system. The reasons may be as follows. (1) PFO is a luminophore and presents an ECL peak at about 1.97 V; (2) PAMAM holds large surface area and activity center, thus could accelerate the electron transfer rate; (3) C_{60} could amplify the ECL signal of PFO due to the fact that C_{60} could accelerate the electron transfer in ECL reaction.

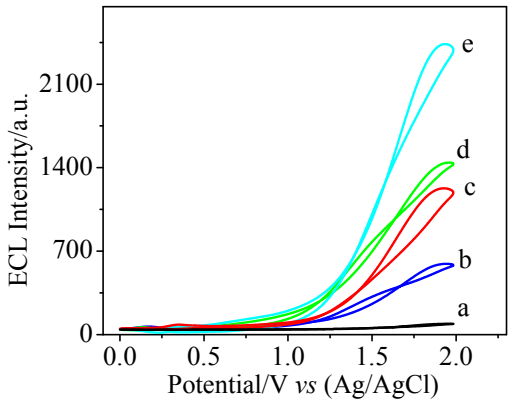

223

224 **Fig. S7** ECL profiles of (a) GCE, (b) PFO/GCE, (c) C_{60}-PFO/GCE, (d) PAMAM-PFO/GCE and

225 (e) C_{60}-PAMAM-PFO/GCE in 0.10 M PBS (pH 7.0) containing 4.50×10^{-7} M H_2O_2.

226 **Table S1** Comparison of different non-enzymatic sensors for the determination of H_2O_2.

Electrode materials	Determination method	Linear range	Detection limit	Reference
AuCu Nanowires	Amperometry	5.0 nM-360 nM 360 nM-440 μM	2.0 nM	3
Core/Shell Au/MnO	Amperometry	20 nm-100 nm	8.0 nm	4
Goldnanocoral	ECL	0.1 μM-100 μM	30 nM	5
Co_3O_4-rGO	Amperometry	0.015mM-0.675 mM	2.4 μM	6
GQDs/AgNPs	Colorimetric	0.1 μM-100 μM	33 nM	7
ZnSe QDs	ECL	0.61 μM-310 μM	0.2 μM	8

C_{60}-PAMAM-PFO	ECL	2.30 nM-8.05 mM	0.61 nM	This work

2.4 Analytical application of the sensor in serum samples

The analytical reliability and potential application of ECL biosensor was evaluated by a standard addition method. Human serum samples were diluted with pH 7.0 PBS and the results of standard addition method were shown in Table S2. The recoveries ranged from 94.7% to 103%, confirming that the proposed biosensor could be reasonably applied in human serum samples.

Table S2 Recoveries of choline at the biosensor in human serum samples.

Sample	c_{Added}/μM	c_{Found}[a]/μM	Recovery/%
1	0.150	0.142±0.005	94.7
2	0.250	0.257±0.014	103
3	0.350	0.341±0.006	97.4
4	0.450	0.447±0.028	99.3

1 C. F. Wu, B. Bull, C. Szymanski, K. Christensen and Jason McNeill, *ACS NANO*, 2008, **11**, 2415-2423.

2 Q. Wang, Y. Song, H. Xie, Y. Q. Chai, Y. L. Yuan, R. Yuan, *Chem. Commun*., 2015, **51**, 1255-1258.

3 N. Wang, Y. Han, Y. Xu, C. Z. Gao and X. Cao, *Anal. Chem*., 2015, **87**, 457-463.

4 H. Y. Zhu, A. Sigdel, S. Zhang, D. Su, Z. Xi, Q. Li and S. H. Sun, *Angew. Chem*., 2014, **126**, 12716-12720.

5 M. Xu, W. J. Qi, L. Zhang, J. P. Lai, A. Rehman, S. Majeed and J. B. Xu, *Microchim Acta*., 2014, **181**, 737-742.

6 L. J. Kong, Z. Y. Ren, N. N. Zheng, S. C. Du, J. Wu, J. L. Tang and H. J. Fu, *Nano Research*., 2015, **8(2)**, 469-480.

7 Chen, S., Hai, H., Chen, X.W., and Wang, J.H., *Anal. Chem*., 2014, **86**, 6689-6694.

8 X. F. Hu, H. Y. Han, H. J. Hua, Z. H. Sheng, *Biosens. Bioelectron*., 2010, **25**, 1843-1846.